Evaluation of Photocatalytic Activity of Fe Doped Tio_2 Thin Film Prepared by Sol-Gel Hot Dip-Coating

S. Naghibi[a,*], Sh. Vahed[b], O. Torabi[c]

[a] *Department of Metallurgy and materials engineering, Shahreza Branch, Islamic Azad University, Isfahan, Iran.*
[b] *Department of Food Science, Shahreza Branch, Islamic Azad University, Isfahan, Iran.*
[c] *Advanced Materials Research Center, Najafabad Branch, Islamic Azad University, Isfahan, Iran.*

ARTICLE INFO

Article history:

Received 29 May 2014
Accepted 29 Jun. 2014
Available online 31 Aug. 2014

Keywords:

Fe doped TiO_2
Thin film
Photocatalytic properties
Hot–dip coating
Sol–gel

ABSTRACT

Application of Fe–TiO_2 photocatalysis using sol–gel method by hot–dipping technique was investigated. The influences of fabrication parameters; molar ratios of Fe to TiO_2, the sol temperature, poly ethylene glycol (PEG) content and the number of dipping cycles on the photocatalytic activity in visible light region were studied. Results revealed that a higher photocatalytic performance of Fe-TiO_2 films could be achieved using the molar ratio of Fe to TiO_2: 0.015, the sol temperature: 70 °C, PEG content: 2 wt. % and 5 dipping cycles. The photodegradation efficiency of this sample after 2 h of visible light irradiation increased up to 80% and no crack was detected on the surface of the thin film. When the sol temperature increased from 25 to 70 ºC (the boiling point of the sol), its viscosity increased due to the presence of PEG via forming cross linkage. This phenomenon resulted in the change of the coating microstructure and the improvement the optical properties.

1. Introduction

Antifog, antireflective, antiglare and antibacterial coatings are some types of optical coatings applied to the surface of glassy pieces and other optical devices to improve their performances. The coating agents play a significant role in the properties of the coated glass. Magnesium fluoride (MgF_2) is often used for reducing the surface's reflection coefficient [1]. TiO_2 is the most famous antifog agent due to its highly hydrophilic behaviour under ultra violet (UV) light [2].

The antibacterial glass is more demanding in several applications such as in buildings, food packing, medical laboratories, etc. This property has been developed by applying TiO_2 photocatalyst on the surface of glass to enhance the photocatalytic effect in the UV region. However, the need for a UV source limits its benefits. To deal with this problem, a generic way is to modify TiO_2 by doping with a metal ion and/or an organic polymer, which leads to a decrease in band gap energy; therefore, photo excitation could occur in visible and/or UV light. The most popular dopants for this purpose are Ag, Fe, V, Au, Pt and etc., which have been doped by many production methods, including ion–assisted sputtering, plasma, ion–implantation, chemical vapour deposition (CVD), and sol–gel [3]. However, a sol–gel process is considered as one of the most promising techniques due to fewer types of

Corresponding author:
E-mail address: naghibi@iaush.ac.ir (Sanaz Naghibi).

equipment, and hence potentially lowers costs. Moreover, the most important advantage of sol–gel process over other methods is the ability to control precisely the microstructure (pore volume, pore size, and surface area) and composition (stoichiometry) of the products [4]. During the sol–gel process, prior to gelation, the sol could be applied as a thin film by dipping or spinning processes [5, 6].

TiO_2 is a good ceramic material and can be used as a permanent antibacterial coating that has attracted much attention of researchers due to its significant optical, electrical, and photoelectrochemical properties. So far, a number of experimental researches have been successfully conducted in the field of the properties of TiO_2 films. Sonawane et al. prepared a thin film of Fe–TiO_2 on a substrate. The addition of Fe into the sol showed excellent photocatalytic activity. Up to 95% of methyl orange can be decomposed in sunlight within 34 h [7]. In addition, Sonawane et al. applied Au–TiO_2 thin film to degrade phenol in sunlight. By doping Au into the TiO_2 structure, its photo response under visible light increased by more than 20 times, and its absorption wavelength shifted from 340 nm in UV to 450 nm in the visible region [8]. As it is well documented by Zhao et al., the photocatalytic efficiency of Fe–TiO_2 can be increased to 98% compared to that of the undoped one [9]. On the other hand, Moujoud et al. used hot–dip coating process to fabricate thin films. This technique seems to be a good method to control the morphology and thickness of the sol–gel films by varying the drawing temperature [10].

Following our attempts to eliminate the crack formation, the TiO_2 thin films have been deposited by sol-gel dipping technique on stainless steel. The sol used contains poly ethylene glycol (PEG) as a major constituent to improve the sol stability, the surface roughness and the green adhesion [5].

In the present work, sol–gel dipping technique was applied to form nanocrystalline Fe doped TiO_2 thin film on a glass substrate. In this regard, PEG was added to the sol. The sol temperature, the PEG content and the number of dipping cycles were investigated to optimize the morphology and photocatalytic behaviour of the Fe doped TiO_2 thin film.

2. Experimental

2. 1. Starting materials

Titanium tetra isopropoxide (TTIP, >98%, Merck Co., Germany) as a Ti source, ferric nitrate ($Fe(NO_3)_3.9H_2O$, Merck) as a Fe precursor, isopropyl alcohol (iPrOH, >99.5%, Merck Co.) as a solvent, hydrochloric acid (HCl, 37%, Merck Co.) and triethylamine (TEA, 99%, Merck Co.) as reagents to adjust pH, distilled water as a hydrolytic agent, and PEG (average molecular weight: 6000 g, Merck Co.) were used as the starting materials.

2. 2. Experimental Design

In this study, an experimental plan is established to optimize the photocatalytic behaviour of the Fe doped TiO_2 films prepared by sol–gel dipping technique under various deposition parameters, i.e. Fe amount, sol temperature, the PEG content, and the number of dipping cycles. The aim of this work is the optimum deposition conditions for high photocatalytic properties in visible light. The input parameters and the steps of experiments are shown in Table 1. As can be seen, three different steps are defined to investigate the influences of variables on the properties of the coated samples.

2. 2. 1. First step; Preparation of the Fe–TiO_2 nanoparticles to optimize the Fe content

Fe–TiO_2 sol was prepared by mixing TTIP, iPrOH, H_2O with adequate amounts of $Fe(NO_3)_3.9H_2O$ (according to Table 1). The molar ratios of the iPrOH /TTIP and H_2O/iPrOH were 50 and 4, respectively. The solution was stirred continuously at room temperature. Given that in Ti^{4+}–containing sol, the hydrolysis does not occur in pH more than 1.75 [11], to decrease the pH value to 1.5, HCl was added to the solutions and was continuously stirred for 24 h. In this step, 1 wt. % of PEG was added to the samples and continuously stirred for 24 h. To increase the pH value of the solution to 9, adequate amounts of TEA were dropped into the stirring solutions. After filtering and repeated washing (3 times with distilled water), the prepared precipitates were dried at 70 ºC for 24 h. The dried powder was fired in a laboratory electrical furnace at a heating rate of 10 ºC/min

Table 1. Preparation variables and conditions of the samples

Experimental steps	Variable	Values of the variable	Samples	Tests
First step	Fe content	Molar ratio of Fe to TiO_2 = 0, 0.005, 0.015 and 0.03	F1: 0 F2: 0.005 F3: 0.015 F4: 0.03	XRD, EDS, UV visible spectroscopy
Second step	sol temperature	Ambient, 70ºC	S1: 25 ºC S2: 70 ºC	EDS, UV visible spectroscopy (photodegradation of MB)
Third step	PEG content	0, 1 and 2 wt.%	T1: 0 PEG, 3 layers T2: 1 PEG, 3 layers T3: 2 PEG, 3 layers T4: 0 PEG, 5 layers T5: 1 PEG, 5 layers T6: 2 PEG, 5 layers	UV visible spectroscopy (photodegradation of MB), SPM, FESEM, EDS
	number of dipping cycles	3 and 5		

and the soak time of 2 h at 500 ºC. The calcined powder samples (F1–F4) were investigated by X–ray diffraction (XRD) analysis, energy dispersive spectroscopy (EDS), and UV–visible spectroscopy to evaluate the optical properties.

2. 2. 2. Second step; Preparation of the Fe–TiO_2 thin films to optimize the sol temperature

At this step, Fe–TiO_2 sol was prepared as described before in section 2.2.1. According to the results obtained in the first step, the optimized condition to prepare the Fe–TiO_2 sol would be specified. At this step, three layers of Fe–TiO_2 thin films were deposited on the clean glass substrates by sol–gel dip coating method at a withdrawal speed of 100 mm/min and held for 1 min by a dip coater (109C, Pasargad Nano Equipment, Tehran, Iran). As can be seen in Table 1, the variable in this step was the sol temperature; therefore, deposition process was done at two temperatures: 25 ºC (ambient temperature) and 70 ºC (boiling temperature of the sol). The samples were prepared under the same calcination conditions mentioned for the first step. Photocatalytic properties of the samples S1 and S2 were evaluated by measuring the photodegradation of methylene blue (MB) in aqueous solution after 0, 30, 90 and 135 minutes of irradiation.

2. 2. 3. Third step; Optimization of the PEG content and the number of dipping cycles

At this step, the Fe–TiO_2 sol was prepared as described in section 2.2.1 and deposited on the clean glass substrates under the same conditions with the second step. In accordance with the results of the first and second steps and Table 1, six samples were prepared (see Table 1, samples T1-T6). The variables were PEG content (0, 1 and 2 wt. %) and the number of dipping cycles (3 and 5 cycles). The other parameters were chosen in accordance with the results of the previous sections (molar ratio of Fe to TiO_2 = 0.015 and the sol temperature = 70 ºC). Photocatalytic properties, microstructure, and topographic features of the coated glass samples were compared to determine the best conditions (the PEG content and the number of dipping cycles). The photocatalytic activity of the films under visible light irradiation for 2 h was evaluated by measuring the degradation of absorbance for an MB aqueous solution. The chemical microanalyses of the samples were performed by EDS.

2. 3. Characterization

The optical characterization of the sols (F1-F4) was carried out using UV–visible spectrophotometer (T70, PG Instruments Ltd., England) in the wavelength range of 200 to 800 nm. To compare the absorption of different samples, the area under the absorbance vs. wavelength (λ) curves was measured and determined.

X–ray diffraction (XRD) analysis was carried out by X–ray diffractometer (D8 advance, Bruker, Germany) using Cu tube anode (K_α = 1.540598) and Ni filter. PANalytical X'Pert HighScore software was also used for the analysis of different peaks. The diffraction

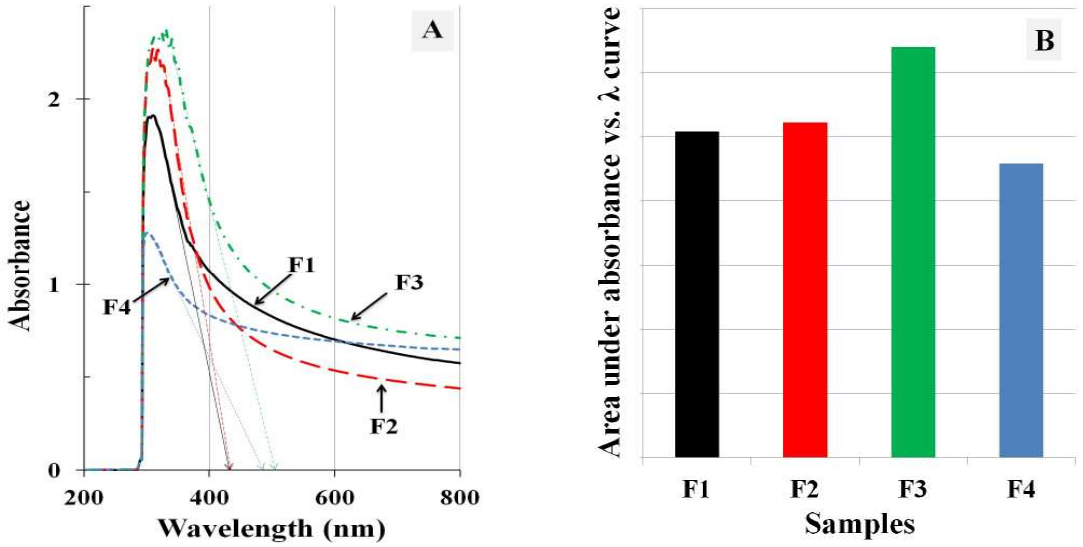

Fig. 1. (A) UV–visible absorption spectra of F1–F4 samples, (B) Absorbance of the samples by measuring the area under the absorbance *vs.* λ curves

patterns of the products were compared with the proposed standards by the joint committee on powder diffraction and standards (JCPDS).

Lattice strain and the crystallite size of the specimens were calculated from the broadening of the XRD peaks using the Williamson–Hall method [12] according to equation (1).

$$B \cos\theta = (0.9\,\lambda / d) + \eta \sin\theta \quad [1]$$

Where d, θ, λ, η and B are crystallite size, diffraction angle, wavelength of the X–ray ($\lambda_{Cuk\alpha1}$=1.540598 Å), lattice strain, and the peak full width at half maximum (FWHM), respectively. Thus, when "B.cosθ" is plotted against "sinθ" (for the main peaks of each XRD pattern), a straight line is obtained with the slope as lattice strain (η). The qualitative assessment strain based on peak broadening could be calculated according to the drawn diagram.

Morphology of the deposited layer was studied by field emission scanning electron microscopy (FESEM, 4160, 15 kV; Hitachi, Japan), and the surface topography was characterized by scanning probe microscopy (SPM, Dualscop C–26, DME, Germany).

The photocatalytic activities of the coated samples were evaluated by measuring the decomposition rate of MB at room temperature. In each experiment, 10 mL of aqueous MB solution (4 mg/L) was poured into the Petri dish, and a coated substrate was placed in it. Then, it was irradiated with the visible light (two fluorescent lamps, 18 W, Philips). The light wavelength of the fluorescent lamp is mainly located between 420 nm and 670 nm. The distance between the light source and the surface of the suspension was 10 cm. Then, the changes of MB concentration vs. time were measured by a UV–visible spectrophotometer at 664 nm. The degradation rate constants (k, min^{-1}) were measured from the slopes of ln (C_0/C) vs. irradiation time (t) curves, presuming a first order kinetics at this stage of the reaction (where C_0 and C are the concentrations of MB at the initial time and at the time t, respectively).

The Fe and Ti contents of the calcined powder as well as the thin films were estimated by using EDS technique.

3. Results and Discussion

3. 1. *First step; Effect of Fe addition on the optical properties and phase components*

The main aim of doping Fe into TiO_2 structure was to shift the absorption edge towards the visible region of the light spectrum to gain the photoexcitation phenomenon without UV requirement. Different Fe contents were appraised to modify the TiO_2 structure. Fig. 1–A depicts the UV–visible spectra of the suspensions prepared by using sol containing different concentrations of Fe (the molar ratios of Fe to TiO_2 for samples F1–F4 were 0, 0.005, 0.015 and 0.03, respectively), and Fig 1-B shows the area under the absorbance vs. λ curves.

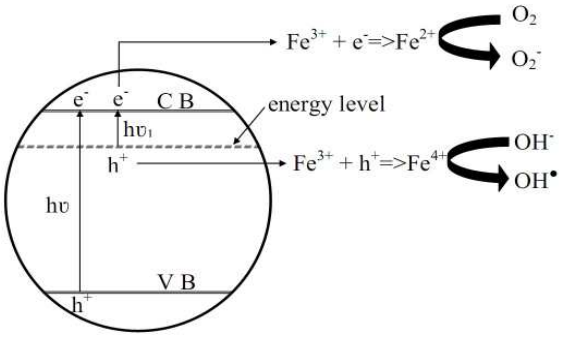

Fig. 2. Processes involved in Fe-doped TiO_2 particles upon band gap excitation. CB: Conduction Band, VB: Valence Band.

As can be seen, the pure TiO_2 sol showed absorption in the UV region. However, the sols prepared by addition of Fe show different behaviours. In curves F2 and F3 the absorption edges of TiO_2 show a red–shift, whereas in curve F4, the absorption edge **exhibited no considerable change.** The addition of the dopant shows not only shifting in the absorption edge but also varying the absorption of the sols in the whole UV–visible range (200–800 nm). Broadening the light absorption zone towards the red region and also increasing the area under the absorbance vs. λ curves could make the doped samples able to absorb light in the visible region.

Fig.1–B illustrates the sum of the absorbance values in the wavelength range of 200–800 nm, indicating the influence of Fe additions on the optical properties of the sols. According to this figure, the amount of absorbance by addition of Fe to TiO_2 increases to a maximum value and then decreases. This was also reported before by Kernazhitsky et al. [13]. The photocatalytic activity of TiO_2 depends on competition between the rate of transferring surface charge carriers and the recombination rate of electrons and holes. Oxygen plays a substantial role in this process by trapping electrons in the conduction band and hindering electron–hole recombination [14]. By Fe ion doping into TiO_2 structure, three features Fe^{2+}, Fe^{3+} and Fe^{4+} can be obtained, in which Fe^{3+} is known as the most stable form. The holes and electrons are generated under irradiation [equation (2)], then Fe ions trap them. Therefore, Fe^{2+} and Fe^{4+} are formed [equations (3) and (4)] and transferred to the catalyst surface; so, they release holes

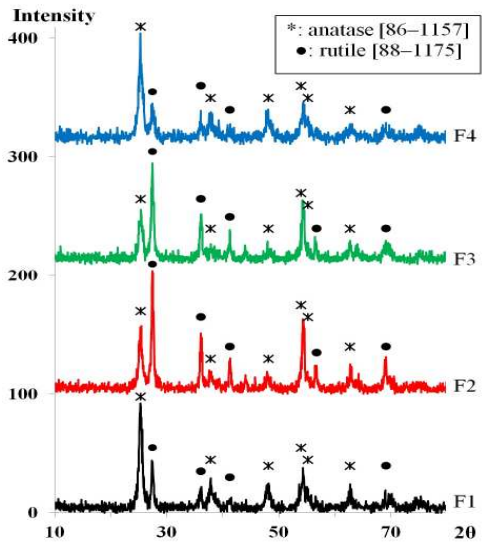

Fig. 3. XRD patterns of the samples, the asterisks refer to anatase [86–1157] and the circles show the main peaks of rutile [88–1175].

and electrons. In this step, Fe^{3+} appears again [equations (5) and (6)], along with hydroxyl radical ($OH^•$) and hyperoxide (O_2^-) [13, 9]. The photocatalytic mechanism is schematized in Fig. 2.

$TiO_2 + h\nu => h^+ + e^-$ [2]

$Fe^{3+} + h^+ => Fe^{4+}$ hole trapping [3]

$Fe^{3+} + e^- => Fe^{2+}$ electron trapping [4]

$Fe^{+4} + OH^- => Fe^{3+} + OH$ hole release [5]

$Fe^{2+} + O_2 => Fe^{3+} + O_2^-$ electron release [6]

It is worth mentioning that Fe as a dopant could affect TiO_2 optical behaviour by (a) shifting the absorption edge, (b) varying the absorbance, (c) hindering the recombination and (d) providing the recombination centres. On the other hand, it could influence (e) the degree of crystallinity, (f) lattice strain and (g) phase component. These items lead to the fact that the influence of Fe doping on the TiO_2 properties is directly affected by its dosage. Fig. 1–B confirmed the relation between Fe concentration and absorption. By adding a small amount of Fe (F2 sample, see Table 1), the absorbance increased gradually, while by continuously increasing the Fe concentration (F3), and the absorbance increased rapidly. More increase in the Fe content (F4), the absorbance decreased rigorously. This is because when a little amount of Fe is present (F2), it behaves as an electron scavenger. Fig. 3 shows the XRD patterns of these samples and Table 2 presents the phase

Table 2. Phase component and lattice strain values of first step samples

Data sources	Sample codes		F1	F2	F3	F4
XRD	Lattice strain (%)		0.4932	0.5356	0.5562	0.8740
XRD	Crystallite size (nm)		10.962	12.958	11.964	8.009
XRD	Phase (%)	Anatase	~ 70	~ 25	~ 20	~ 75
		Rutile	~30	~ 75	~ 80	~ 25
EDS	Atom (%)	O	66.33	66.5	66.3	66.0
		Ti	33.21	33.1	33.0	32.5
		Fe	0	0.13	0.44	0.90

component (XRD), elemental compositions (EDS) and lattice strains (XRD). Fig. 3 illustrates that the main phase is anatase, whereas rutile is the dominate phase in F2 and F3 samples. This notion approves that crystallization occurred well in these samples, in addition to anatase phase; peaks corresponding to rutile were also detected, due to the anatase to rutile conversion because of the presence of Fe. However, in the undoped sample (F1) this anatase to rutile transformation took place only due to the firing temperature. From the curves of F2 and F3 of the pattern it can be seen that rutile peaks are more intense which means that the increase in Fe content promotes anatase to rutile transformation. The sample with the highest amount of Fe (curve F4 in Figure 3 contains more anatase, suggesting that the transformation of anatase to rutile is inhibited or slowed down due to the presence of more Fe content. This may be because in Fe/TiO_2 synthesized by sol–gel technique the Fe ions are adsorbed on TiO_2 oligomers and as the concentration of metal ions increases, the ion density of Fe around a TiO_2 nanoparticle increases. This limits the particles to join each other; as a result, the smaller diameter particles are shaped (this is supported by the values of the crystallite size, see Table 2). Since the anatase phase is most stable at low particle dimension [8], the formation of rutile will not be dominated.

Considering Fig. 1and 3, Fe plays an important role in shifting the absorption edge, and could increase the absorption by changing the phase component and hindering the recombination in TiO_2 structure. Although the Fe content of F4 was higher than the others, its absorption edge shifting and absorbance were less than those of F3, because of providing the recombination sites and in anatase amount.

According to Table 2, by increasing the Fe content, lattice strain was found to increase, as a result of appearing the lattice defects. Moreover, it can be observed that the average grain size increased and achieved its maximum value (12.958 nm for F2 sample) by Fe doping. More increase in the dopant content caused the decrease in the crystallite size which was discussed before.

The EDS data of Fe/TiO_2 nanoparticles (see Table 2) confirm the existence of the Fe atoms in the solid powder samples (F2, F3 and F4) but the XRD patterns do not show any traces related to Fe (even for F4). Therefore, it may be concluded that the Fe ions are uniformly dispersed among the as-synthesized crystallites.

In the first step, although F4 samples contained anatase as the main phase but the best photodegradation responses were achieved in F3 sample; so, its preparation condition would be used to modify the as–synthesized TiO_2 nanoparticles at the next steps.

3. 2. Second step; Effect of the sol temperature on the optical properties of the as–prepared thin films

The variable of this step is the sol temperature. To choose one sample as the best, the photocatalytic activities of S1 and S2 (see Table 1) were evaluated by degradation of MB solution under visible light irradiation. Fig. 4 plots the ln (C_0/C) *vs.* irradiation time (t) curves

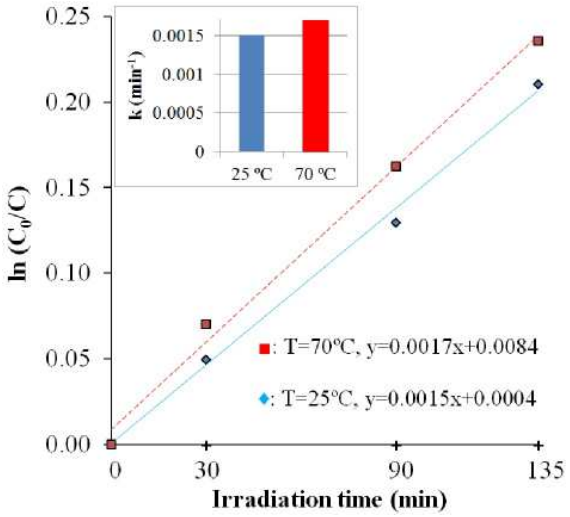

Fig. 4. Kinetics of the photocatalytic degradation of MB solutions (♦) S1 and (■) S2, the apparent rate constants (k, min^{-1}) of degradation of MB were illustrated in the inse.

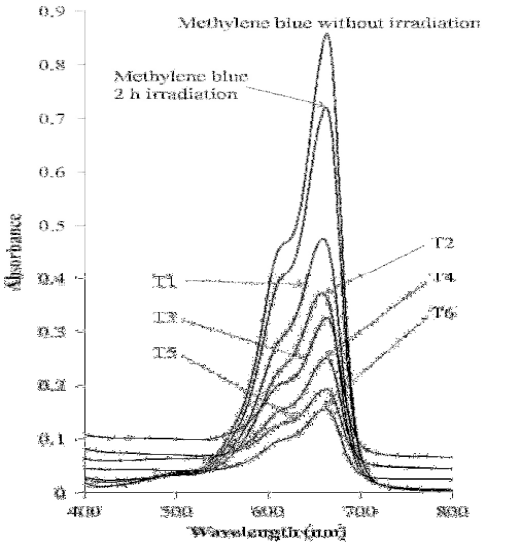

Fig. 5. UV–visible absorption spectra of the photocatalytic degradation of MB solutions due to T1–T6 samples photoactivated after 2 h visible light irradiation, accompained by that of the MB suspention without and with 2 h visible light irradiation

and the degradation rates are illustrated in its inset. This figure indicates that the first order of dye removal kinetic is acceptable for both samples, but comparison of the lines slop reveals that $k_{S2} > k_{S1}$. Photocatalytic activity of TiO_2 thin layers is severely affected by the crystallite size, surface area and pore structure. Smaller crystallite size, higher surface area, and larger pore volume are noted to have positive effects on the photocatalytic activity [15]. These characteristics could be achieved by controlling the deposition parameters such as the withdrawal speed, substrates temperature, conditions of sol, etc. When the sol temperature increased from 25 to 70 ºC and other parameters were kept constant, the photocatalytic activity improved. It seems that this phenomenon is very sensitive to the sol viscosity accessed with the increase in the sol temperature. This is exactly the opposite of that reported by Vorotilov et al. [16]. The appeared antithesis probably refers to the starting materials, and particular attention is paid to PEG. The viscosity of the sol can increase with the addition on of polymers and raising the temperature [17]. This is because of the thermoreversible behaviour of the PEG solution, gelated when heated due to the formation of cross linkage.

In accordance with the EDS results, by increasing the sol temperature from 25 to 70 ºC (samples S1 and S2), the atomic percentage of Fe can increase from 0.40 % (related to S1) to 0.49 % (related to S2). As a result, an increase in the amount of the doped Fe into TiO_2 structure leads to the improvement of the photocatalytic properties.

Here, the viscosity of the sol increased at 70 ºC; so, the Fe content in TiO_2 structure and the photocatalytic activity of the thin film improved. For that matter, S2 was chosen as the best in this step and its preparation conditions would be used in the next step.

3. 3. Third step; Optimization of the PEG content and the number of dipping cycles

Fig. 5 illustrates the UV–visible spectra of the Fe–TiO_2 coatings prepared by hot–dip coating method in different deposition conditions (see Table 1).

To compare the influences of Fe–TiO_2 thin films (T1–T6) on the degradation of MB, the intensity of the main peak of absorbance (at ~ 660 nm) was measured. As can be seen, 2 h visible light irradiation to MB suspension caused ~ 17 % decrease in its concentration due to photodegradation of the dyes. While the MB suspension was poured onto the coated glass and exposed to visible light, the absorbance

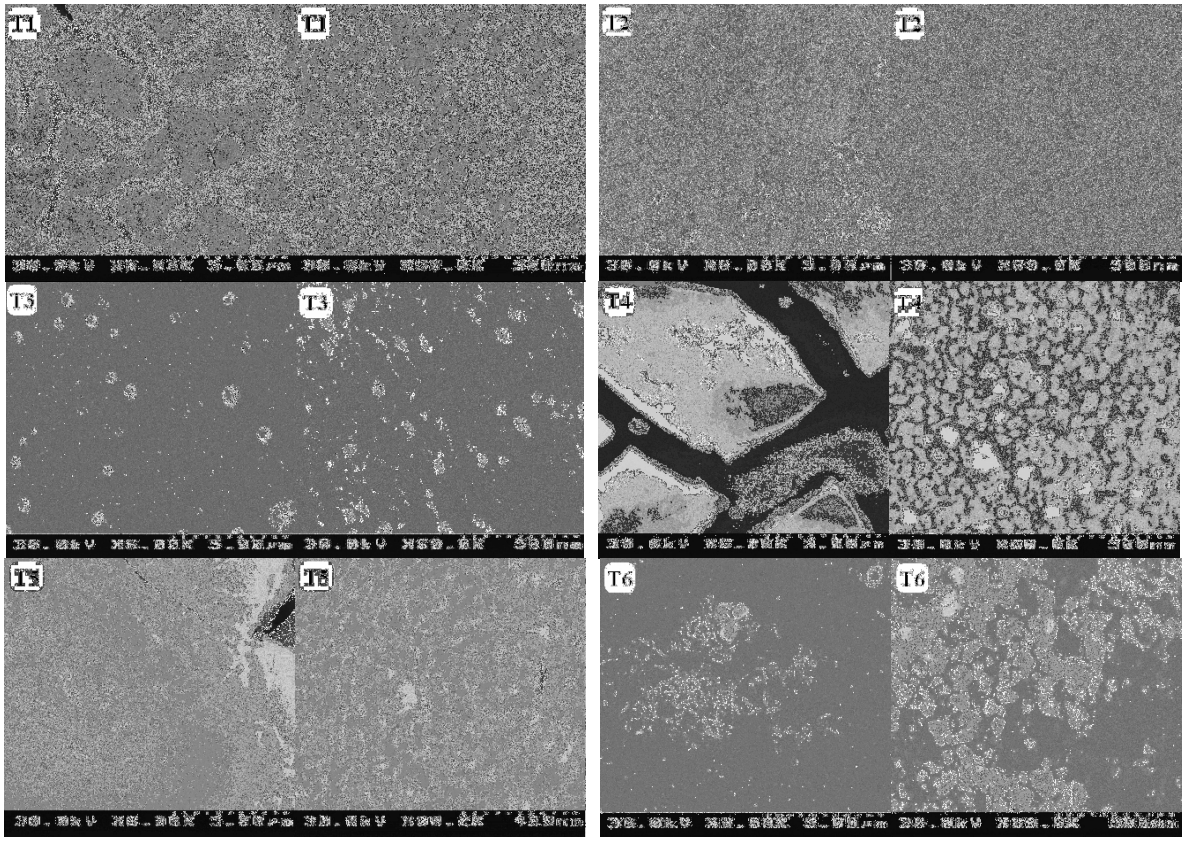

Fig. 6. FESEM images of T1–T6 samples with 6.000 and 60.000 magnitudes

Table 3. Roughness values and atomic percentage of Fe in T1–T6 samples.

Samples	T1	T2	T3	T4	T5	T6
Roughness (nm)	212	145	165	179	137	154
Atomic % of Fe	0.47	0.49	0.48	0.46	0.48	0.50

especially at ~ 660 nm decreased abruptly (40–80%), which might be due to the photocatalytic activity of the coated samples.

The number of dipping cycles of samples T1, T2 and T3 was three, whereas the amount of PEG were 0, 1 and 2 wt. %, respectively. As can be seen in Fig. 5, by using T1 sample (PEG free), the photocatalytic activity was minimum, and about 40% of MB was decomposed. The addition of 1 and 2 wt. % of PEG (T2 and T3) increased the photocatalytic activity of the catalysts, and 54% and 62% of the MB were decomposed, respectively. The addition of PEG into the sol affects the topography and microstructure of the films due to its influences on the sol viscosity and adherence behaviour [7]; therefore, its increase causes an increase in the grain size, and the matrix shows a smoother appearance [5]. Fig. 6 and 7, which illustrate SEM and SPM images, respectively, confirm the above matter. SEM micrographs (Fig. 6) exhibit that with an increase in the PEG amount, the grains become larger. The calculated roughness values from SPM results concluded in Table 3 show that by adding PEG, the surface roughness parameter decreases. This fact can be attributed to the adhesion nature of PEG. It is known that PEG molecules adsorb exothermically onto TiO_2 oligomers by forming hydrogen bonds between oxygen atoms in the PEG and hydroxyl groups on the TiO_2 oligomers [18]. Sonawane et al. [8] suggested that the hydroxyl content of the films increases with respect to the increase in added

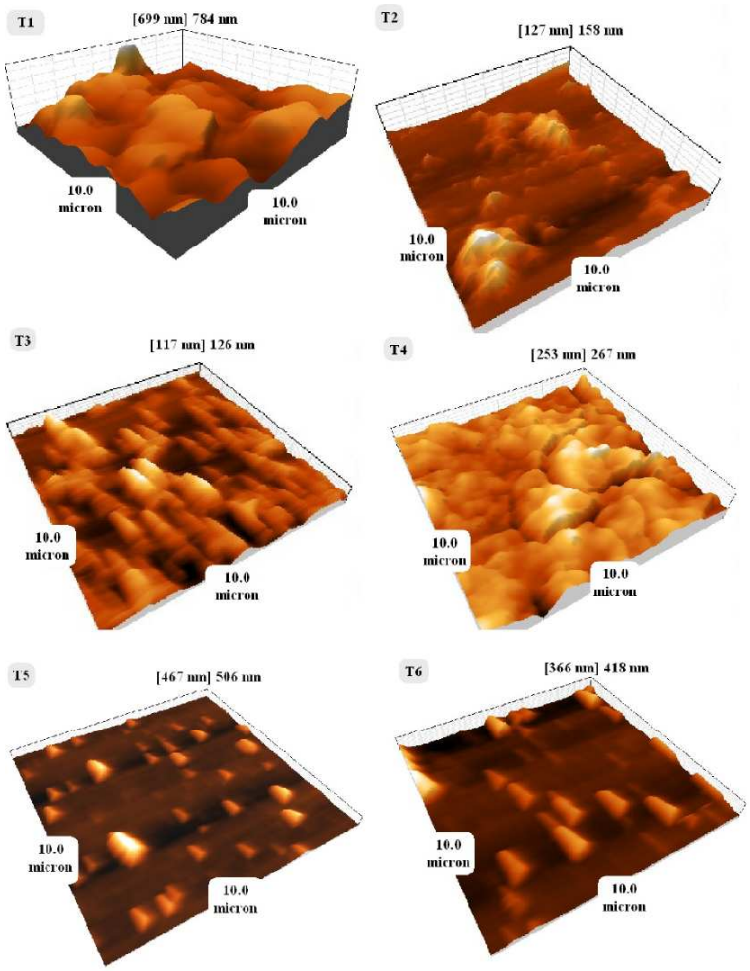

Fig. 7. 3D SPM images of T1–T6 samples

PEG. Vijay et al. [19] showed that one of the most important factors influencing phtocatalytic activity of TiO_2 is the amount of hydroxyl group. Furthermore, the more the number of pores [8] and the higher surface area [20], the more the photocatalytic activity of the films.

Fig. 5 displays that the influence of the PEG content on the optical behaviour of T4, T5 and T6 was similar to that of T1, T2, and T3. In addition, the photocatalytic activity can be affected by changing the number of dipping cycles. By comparing the roughness values (see Table 3) of PEG–free samples (T1 and T4), 1 wt. % PEG containing samples (T2 and T5), and 2 wt. % PEG containing samples (T3 and T6), it is clear that by increasing the dipping cycles from 3 to 5, the roughness parameters decrease, which is in good agreement with the results of our previous work. More narrow range of particle size and homogeneous surface structure are obtained by arising dipping cycles and hence, the roughness value decreases [5]. On the other hand, the results of Fig. 5 show that the photocatalytic activity of the coated samples was promoted with an increase in the number of layers. Notwithstanding lower roughness (Table 3) and higher grain size (Fig. 6); because of higher number of dipping cycles (see Table 1) of samples T4, T5 and T6, their photocatalytic activity is higher than that of T1, T2 and T3, respectively. This phenomenon can be related to the concentration of the photocatalyst deposited on the substrate. The more the layers of deposited film, the more the number of pores generated during calcinations; therefore, the formed hydroxyl content increases. While this photocatalysis sample is exposed to light, electrons and holes are formed. The holes and hydroxyl ions combine

and result in hydroxyl radicals which encourage the photocatalytic activity [7].

Three–dimensional (3D) SPM images of the samples are presented in Fig. 7. As can be seen, some abnormal triangular–like grains appear in T3, T5, and T6 samples. One can find traces of these grains in SEM images in cubic form (see Fig. 6). It should be noted that the dimensions of these grains are ~ 500 nm according to SEM and SPM images, leading to an increase in both roughness parameters and the specific surface area. One possible reason for this phenomenon could be that the particles are prone to join each other and higher diameter particles are shaped by increasing the PEG amount and the number of dipping cycles (images of samples 3, 5, and 6 in Fig. 7).

Obviously, the presence of the entirely shielding TiO_2 film will diminish the accessibility of the irradiated light to the glass surface, whereby causing a promotion in the photocatalytic activation process. As a result, the light scattering is induced by surface and volume imperfections [21]; therefore, a periodic array of micro–cracks exists along the film which could diminish photocatalytic properties. Fig. 6 shows that the use of PEG as an additive prevents the crack formation in samples T2 and T3 (with three layers of thin film), but regarding the five–layered thin film samples (T4, T5 and T6), T6 is the only sample that contains no cracks. It can be concluded that more PEG is required to prevent crack formation by increasing the number of dipping cycles.

The EDS results in Table 3 show that the latter variables (the number of dipping cycles and the PEG content) do not affect the Fe content in TiO_2 coated samples significantly, whereas the microstructure and smoothness of the thin layers specified their optical properties.

The Fe doping caused the increase of photoactivity by improving the light absorption of the TiO_2 in UV-visible region. This phenomenon is related to creation of a new energy level close to the conduction band. Therefore, the required energy for excitation decreased and the produced electron-hole pairs increased.

4. Conclusions

The hot–dipping sol–gel technique was utilized to apply an Fe–TiO_2 thin film on a glass substrate. The optimum processing conditions to achieve the goal of this research, namely a highly photocatalytic activity in visible light region and lowly defected coated samples, were found in a sample with the molar ratios of Fe to TiO_2: 0.015, the sol temperature: 70°C, PEG content: 2 wt. % and the number of dipping cycles: 5. The photodegradation efficiency of this sample after 2 h of visible light irradiation increases up to 80% and no crack was detected on the surface of the thin film.

The optical properties under visible light irradiation improved as the temperature at which the thin films are formed increases. The red shift can be related to the increase in the sol viscosity with increasing the temperature due to the existence of PEG. This phenomenon causes the as–deposited thin film to thicken and the Fe content of nanoparticles in thin film to increase, leading to an improvement in photocatalytic properties.

According to EDS results, among all the parameters studied in this work, the sol temperature has great influence on the Fe content in TiO_2 coated samples.

References

1. J. Aigueperse, P. Mollard, D. Devilliers, M. Chemla, R. Faron, R. Romano, J. P. Cuer, Fluorine compounds, inorganic, in: Ullmann's Encyclopedia of Industrial Chemistry, Wiley–VCH Verlag GmbH & Co. KGaA, USA, 2000.
2. A. Fujishima, K. Hashimoto, T. Watanabe, TiO_2 photocatalysis: fundamentals and applications, BKC Inc., Tokyo, Japan, 1999.
3. A. Zaleska, “Doped-TiO2: A Review Doped-TiO2”, Recent Pat. Eng., vol 2, 2008, pp. 157–164.
4. C. Zuo, M. Liu, M. Liu, Solid oxide fuel cells, in: M. Aparicio, A. Jitianu, L.C. Klein (Eds.), Sol–Gel Processing for Conventional and Alternative Energy, Springer Verlag, New York, USA, 2012, pp. 7–37.
5. S. Naghibi, A. Jamshidi, O. Torabi, R. Ebrahimi, “Application of Taguchi method for characterization of corrosion behaviour of TiO2 coating prepared by sol–gel dipping technique”, Int. J. Appl. Ceram. Technol., 2013, http://dx.doi.org/10.1111/ijac.12077.

6. M. R. Golobostanfard, H. Abdizadeh, “Effect of mixed solvent on structural, morphological, and optoelectrical properties of spin–coated TiO2 thin films”, Ceram. Int. vol. 38, 2012, pp. 5843–5851.
7. R. S. Sonawane, B. B. Kale, M. K. Dongare, “Preparation and photocatalytic activity of Fe–TiO2 thin films prepared by sol–gel dip coating”, Mater. Chem. Phys. Vol. 85, 2004, pp. 52–57.
8. R. S. Sonawane, M. K. Dongare, “Sol–gel synthesis of Au/TiO2 thin films for photocatalytic degradation of phenol in sunlight”, J. Mol. Catal. A–Chem., vol. 243 2006, pp. 68–76.
9. W. Zhao, W. Fu, H. Yang, C. Tian, M. Li, J. Ding, X. Zhou, H. Zhao, Y. Li, W. Zhang, “Synthesis and photocatalytic activity of Fe–doped TiO2 supported on hollow glass microbeads”, Nano Micro Lett., vol. 3, 2011, pp. 20–24.
10. A. Moujoud, M. P. Andrews, S. I. Najafi, “Fabrication of sol–gel optical waveguide by hot–dip coating process”, J. Sol Gel Sci. Technol., vol. 35, 2005, pp. 123–126.
11. C. J. Brinker, G. W. Scherer, Sol–Gel Science; The Physics and Chemistry of Sol–Gel Processing, Academic Press, USA, 1990.
12. G. K. Williamson, W. H. Hall, “X–ray line broadening from filed aluminium and wolfram”, Acta Metallurgica, vol. 1, 1953, pp. 22–31.
13. L. Kernazhitsky, V. Shymanovska, V. Naumov, V. Chernyak, T. Khalyavka, V. Kshnyakin, “Effect of iron–group ions on the UV absorption of TiO2”, Ukr. J. Phys. Opt., vol. 9, 2008, pp. 197–207.
14. D. Beydoun, R. Amal, G. Low, S. McEvoy, “Role of nanoparticles in photocatalysis”, J. Nanopart. Res., vol. 1, 1999, pp. 439–458.
15. J. Liu, T. An, G. Li, N. Bao, G. Sheng, J. Fu, “Preparation and characterization of highly active mesoporous TiO2 photocatalysts by hydrothermal synthesis under weak acid conditions”, Microporous Mesoporous Mater., vol. 124, 2009, pp. 197–203.
16. K. Vorotilov, V. Petrovsky, V. Vasiljev, “Spin coating process of sol gel silicatefilms deposition: Effect of spin speed and processing temperature”, J. Sol Gel Sci. Tech., vol. 5, 1995, pp. 173–183.
17. M. Takeuchi, S. Kageyama, H. Suzuki, T. Wada, Y. Notsu, F. Ishii, “Rheological properties of reversible thermo–setting in situ gelling solutions with the methylcellulose–polyethylene glycol–citric acid ternary system”, Colloid Polym. Sci., vol. 281, 2003, pp. 1178–1183.
18. K. Kajihara, T. Yao, “Macroporous morphology of the titania films prepared by a sol–gel dip–coating method from the system containing poly(ethylene glycol). II. Effect of solution composition”, J. Sol Gel Sci. Technol., vol. 12, 1998, pp. 193–201.
19. M. Vijay, V. Selvarajan, K. P. Sreekumar, J. Yu, S. Liu, P. V. Ananthapadmanabhan, “Characterization and visible light photocatalytic properties of nanocrystalline TiO2 synthesized by reactive plasma processing”, Sol. Energy Mater. Sol. Cell., vol. 9, 2009, pp. 1540–1549.
20. S. Naghibi, M. A. Faghihi Sani, H. R. Madaah Hosseini, “Application of the statistical Taguchi method to optimize TiO2 nanoparticles synthesis by the hydrothermal assisted sol–gel technique”, Ceram. Int., vol. 40, 2014, pp. 4193–4201.
21. H. Bach, D. Krause, Thin Films on Glass, Springer, Germany, 1997, p. 108.